NIR-Laser-Switched In Vivo Smart Nanocapsules for Synergic Photothermal and Chemotherapy of Tumors

Zhouqi Meng, Fang Wei, Ronghua Wang, Mengge Xia, Zhigang Chen, Huiping Wang,* and Meifang Zhu**

Cancer poses a great threat to human health and life. Among cancer therapeutics, chemotherapy has been widely applied, in which the active drug should reach the tumor in vivo at the appropriate concentration, and administration of the drug should then be maintained for the required time to produce the therapeutic effect. To facilitate the delivery and dose control of drugs, advanced stimuli-responsive nanocarriers have recently received a great deal of attention. Stimuli-responsive nanocarriers are able to deliver drugs in response to specific stimuli, either endogenous variations (such as pH,[1] enzyme concentration, and redox gradients[2]) or exogenous stimuli (including temperature,[3] magnetic field,[4] ultrasound intensity,[5] light,[6] and electric pulses[7]). It should be noted that with endogenous variations, the precise control of drug delivery is difficult because of the uncontrollable specific microenvironments and individual differences in the human body.[8] In addition, although the release of drugs with exogenous stimuli in vivo is feasible, it is still difficult to attain precise control of the drug release due to the large-scale area of exogenous stimuli, usually causing undesirable side effects. Therefore, it is worthwhile to further develop drug-release technologies, ideally with more benign side effects.

It is well known that near-infrared (NIR) light can penetrate the skin/tissue to irradiate optically sensitive nanoparticles in vivo.[6,9] Lately, NIR laser-induced photothermal ablation therapy (NIR-PAT) has attracted much interest as a minimally invasive therapeutic methodology for cancers. A prerequisite for the development of NIR-PAT is to obtain photothermal nanoagents (PNs). So far, different kinds of PNs have been developed, including polymer nanoparticles,[10] noble-metal nanomaterials,[11] carbon-based nanomaterials,[12] and semiconductor nanomaterials.[13] Our group has developed several semiconductor PNs, including $Cu_{2-x}S$[14] and WO_{3-x}[15] based nanoagents for the photothermal ablation of cancer cells in vivo. Nevertheless, it should be pointed out that NIR-PAT will cease immediately if the NIR laser irradiation is shut off.

To further improve the therapeutic effects from chemotherapy or NIR-PAT, the combination of chemotherapy and NIR-PAT has attracted increasing attention, and several stimuli-responsive nanocomposites have been investigated, including PN@liposome,[10b,16] PN@silica[17] and PN@polymer,[18] Among these nanocomposites, PN@polymer perhaps represents the most promising one, because the stimuli-responsive behavior of polymers has been demonstrated to be well regulated. For example, the low critical solution temperature (LCST) of polymer nanogels can be varied from 26 to 90 °C.[19] Currently, several kinds of PN@thermal-responsive polymers have been developed, such as polymer-based PN@PNIPAM,[20] carbon-based PN@PNIPAM[21] and noble-metal-based PN@PEG/NIPAM,[18] which can deliver drugs under irradiation of an NIR laser, greatly improving chemo/photothermal therapy. It should be pointed out that for all these stimuli-responsive nanocomposites, the intelligent release (switching off/on) by NIR lasers is not yet well established due to the lack of or inadequacy of intelligent release systems. Therefore, it is still necessary to further develop smart nanocomposites that can be switched off/on controllably by an ex vivo NIR laser for simultaneous photothermal/chemotherapy of tumors.

Here, we describe the design and fabrication of the "smart" MEO_2MA@MEO_2MA-*co*-OEGMA-CuS-DOX composite (abbreviated as **G**-CuS-DOX), which consists of thermosensitive MEO_2MA@MEO_2MA-*co*-OEGMA nanogels (abbreviated as **G**) with an LCST of 42 °C, that serve as the nanocarriers, CuS nanoparticles as the photothermal component, and doxorubicin (DOX) as the anticancer drug (**Figure 1**a). **G**-CuS-DOX nanocapsules allow the application of photothermal therapy and drug release simultaneously, which can be switched off/on by an ex vivo NIR laser (**Figure 2**a). Subsequently, nanocapsules were injected into the tumor and close to cancer cells. Under irradiation with a 915-nm laser, cancer cells can be efficiently destroyed; both the tumor growth and metastasis lesions in liver tissue showed significant inhibition, indicating the excellent Synergic photothermal/chemotherapy effects compared to photothermal therapy or chemotherapy effect alone.

The synthesis of **G**-CuS-DOX nanocapsules consisted of four steps, as demonstrated in Figure 1a. The first step was to prepare a thermosensitive MEO_2MA nanogel (abbreviated as **M**) by a simple polymerization reaction (step 1 in Figure 1a).[18b] **M** exhibits an average hydrodynamic diameter of ≈90 nm (Figure S1a, Supporting Information) and an LCST of ≈31 °C (Figure S1b,

Dr. Z. Q. Meng, Dr. M. G. Xia,
Prof. Z. G. Chen, Prof. M. F. Zhu
State Key Laboratory for Modification
of Chemical Fibers and Polymer Materials
College of Materials Science and Engineering
Donghua University
Shanghai 201620, China
E-mail: zgchen@dhu.edu.cn; zmf@dhu.edu.cn
Prof. F. Wei, Ms. R. H. Wang, Prof. H. P. Wang
Experimental Research Center
The First People's Hospital
Shanghai Jiaotong University
Shanghai 201620, China
E-mail: tywhp9618@msn.com

DOI: 10.1002/adma.201502669

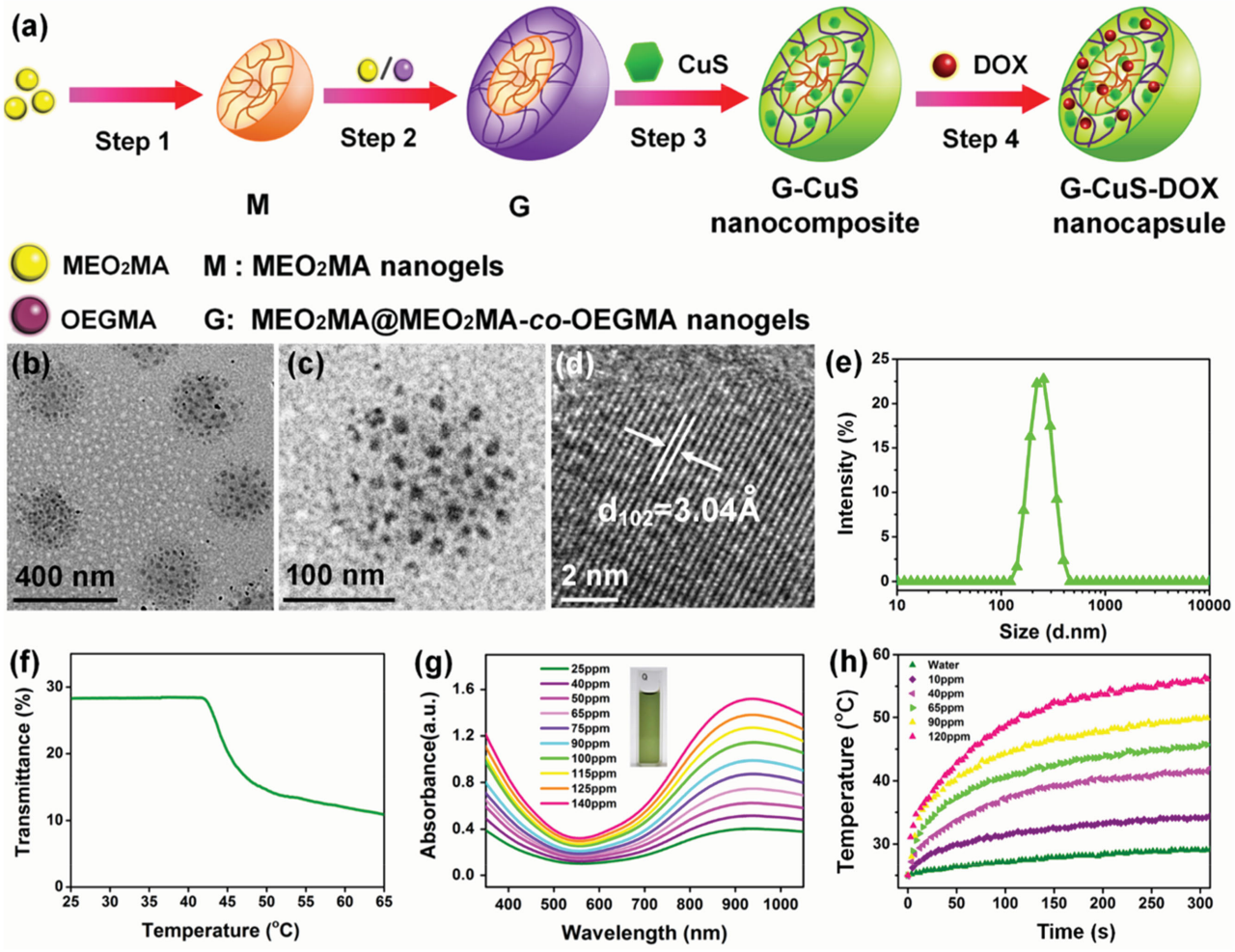

Figure 1. Synthesis scheme and characterization of MEO_2MA@MEO_2MA-*co*-OEGMA-CuS-DOX (**G**-CuS-DOX) nanocapsules. a) Synthesis scheme. b–d) TEM images. e) Size distribution. f) Transmittance versus temperature for a **G**-CuS aqueous dispersion (10 mg mL^{-1}), g) UV–vis absorbance spectra of **G**-CuS dispersions with different Cu concentrations (25–140 ppm). The inset shows a photograph of a **G**-CuS dispersion (10 mg mL^{-1}). h) Temperature curves of **G**-CuS dispersions (Cu concentration: 10–120 ppm) under irradiation with a 915-nm laser (2.0 W cm^{-2}) as a function of time (0–300 s).

Supporting Information).[18b,19a] For in vivo application of thermosensitive nanogels, the LCST must be tuned to a value above the body temperature (>37 °C) but below the hyperthermia temperature (typically, <43 °C) of the photothermal conversion.[18a] In the second step (step 2 in Figure 1a), to adjust the LCST, the *p*(MEO_2MA-*co*-OEGMA) copolymer was used as a shell layer to coat on the **M** seeds, by subsequent seed emulsion polymerization.[18b,19a,b] The resulting MEO_2MA@MEO_2MA-*co*-OEGMA nanogel (abbreviated as **G**) has an average hydrodynamic diameter of ≈254 nm (Figure S1a, Supporting Information) and an LCST of about 42 °C (Figure S1b, Supporting Information). The increases in size and LCST indicate efficient coating of the *p*(MEO_2MA-*co*-OEGMA) copolymer, similar to findings in previous reports.[18b,19b,c] The functional groups of **G** could be deduced from FTIR spectra (Figure S2, Supporting Information).

The third step was the preparation of CuS nanoparticles as photothermal nanoagents in **G** by an in situ co-precipitation method at 80 °C (step 3 in Figure 1a). Figure 1b and 1c show TEM images of the **G**-CuS nanocapsules. Almost no nanoparticles can be found outside of the nanocapsules, while there are some CuS nanoparticles with a diameter of 9.2 ± 3.5 nm that are well dispersed in **G**. This should be attributed to the fact that **G** can simultaneously serve as a nanoreactor and ligand.[18b] The high-resolution TEM (HRTEM) image (Figure 1d) indicates clear lattice fringes, suggesting that the CuS nanoparticle is a single crystal. The interplanar *d*-spacing is determined to be 3.04 Å, agreeing with (102) lattice fringes of a hexagonally structured CuS crystal.[14b] Furthermore, **G**-CuS nanocomposites exhibit an average hydrodynamic diameter of about 274 nm (Figure 1e) and an LCST of about 42 °C (Figure 1f), which is very close/equal to the values measured for **G** (254 nm, 42 °C), indicating that the preparation process of CuS has no obvious adverse effect on the diameter and thermosensitivity of the nanogels.

As a result of their hydrophilicity, **G**-CuS nanocomposites can be well dispersed in water, phosphate buffer saline (PBS), Dulbecco's modified Eagle medium (DMEM), and fetal bovine

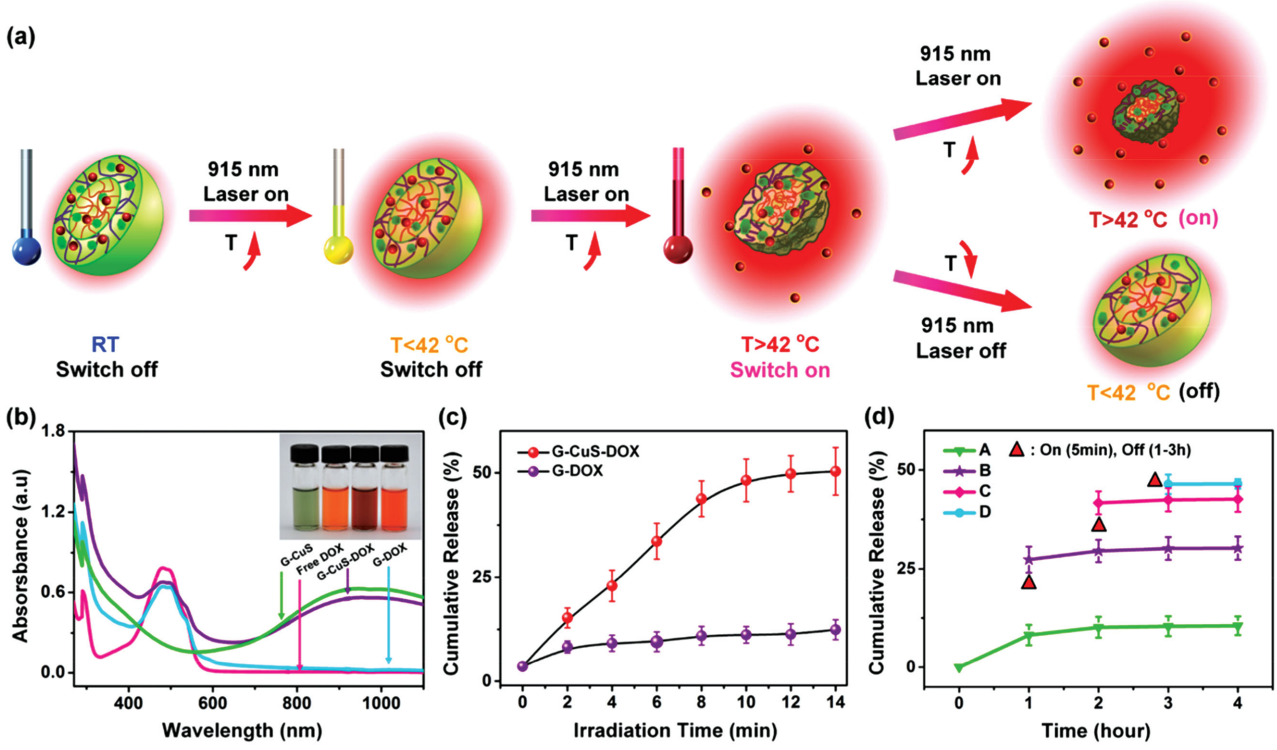

Figure 2. Intelligent DOX release switched "on" or "off" by an ex vivo NIR laser. a) The release scheme. b) UV–vis absorbance spectra of the dispersions containing **G**-CuS, free DOX, **G**-CuS-DOX or **G**-DOX; the inset shows photographs of them. c) Cumulative release of DOX from **G**-DOX or **G**-CuS-DOX under irradiation of a 915-nm laser (2.0 W cm^{-2}) for different times (0–14 min). d) Effects of the irradiation–non-irradiation cycle number (A: 0 times; B: 1 time; C: 2 times; D: 3 times) on cumulative DOX release from **G**-CuS-DOX with the 915 nm laser (1.6 W cm^{-2}, 5-min "on"/55-min "off" for every cycle). The data represent the mean ± standard deviation of triplicate measurements.

serum (FBS) solution. No obvious agglomeration is displayed after storing for several weeks (Figure S3, Supporting Information). The **G**-CuS aqueous dispersions with different Cu concentrations (10–120 ppm, determined by ICP-AES) exhibit a green color (typical, the inset of Figure 1g). Their optical properties are studied by using UV–vis spectroscopy (Figure 1g). The **G**-CuS nanocomposites show enhanced photoabsorption as the wavelength increases from 550 to 950 nm. In particular, the absorption intensity in the NIR region increases linearly with the Cu concentration in nanocapsules (such as, at 915 nm, Figure S4, Supporting Information). Such a strong absorption of **G**-CuS in the NIR region implies a potential for their photothermal conversion upon 915-nm laser irradiation.

Subsequently, the photothermal performance of the aqueous dispersions was investigated under irradiation of a 915-nm laser with an intensity of 2.0 W cm^{-2} (Figure 1h). The blank test demonstrates that the temperature of pure water (or PBS, DMEM, FBS solution without CuS) is only increased by less than 3 °C from the room temperature of 25 °C (Figure S5, Supporting Information). With the addition of **G**-CuS nanocomposites (Cu concentration: 10–120 ppm), the temperature increases dramatically with the increase of the irradiation time from 0 to 100 s, and then remains fairly constant upon further irradiation to 300 s. The temperature elevation (ΔT) at 300 s, which is calculated from Figure 1h, increases almost linearly from 8.5 to 31.3 °C with the Cu concentration from 10 to 120 ppm (Figure S6, Supporting Information). Thus, one can conclude that CuS in the nanocapsules can rapidly and efficiently convert the NIR laser energy into heat, arising from a strong photoabsorption in the NIR region.[14b,15a]

The last step was loading DOX as the model anticancer drug in the **G**-CuS nanocomposites (step 4 in Figure 1a), because the **G**-CuS aqueous solution had a zeta potential of –19.7 mV and could thus absorb positively charged drugs, such as DOX, by electrostatic interactions,[10a,22] forming **G**-CuS-DOX with a zeta potential of –11.3 mV. The original solution of free DOX has a yellow-red color (inset of Figure 2b). The loading of DOX into the nanocarriers changes the color from green **G**-CuS to red-brown **G**-CuS-DOX, or from colorless **G** to red **G**-DOX (the inset of Figure 2b). Their optical properties were also investigated by UV–vis spectroscopy (Figure 2b). The free DOX solution exhibits a typical absorption peak around 480 nm, whereas **G**-CuS-DOX shows both the characteristic absorption peaks from DOX in the visible region and a broad plasma absorption band from **G**-CuS in the NIR region (Figure 2b). Furthermore, both the **G**-CuS-DOX and **G**-DOX solutions show obvious fluorescence quenching compared with the free DOX solution (Figure S7, Supporting Information), which illustrates that DOX is tightly bound to **G**-CuS and **G**,[23] demonstrating the successful loading of DOX. It should be noted that the loading of DOX has no obvious effect on the photothermal properties of CuS, and the **G**-CuS-DOX nanocapsules retain their excellent photothermal performance (Figure S8, Supporting Information). In addition, the DOX loading content (LC_{DOX}, w/w%)

and the encapsulation efficiency (EE_{DOX}, w/w%) are summarized in Table S1, Supporting Information.

To achieve the controllable release of DOX, **G**-CuS-DOX aqueous dispersions (10 mg mL^{-1}, LC_{DOX} = 1%) were continuously irradiated by a 915-nm laser with a power density of 2.0 W cm^{-2} for different times (0–14 min). The solutions were then centrifuged and the concentration of released DOX was determined by UV–vis spectroscopy at 480 nm (Figure 2c). For comparison, the release of DOX from **G**-DOX nanocomposites (without CuS) was also recorded under otherwise identical conditions. The cumulative release of DOX from **G**-DOX is 8.5% at 2 min, and then remains almost unchanged. In contrast, the cumulative release of DOX from **G**-CuS-DOX nanocapsules increases almost linearly from 3.6% (at 0 min) to 43.7% (at 8 min), then exhibits a slow increase to 50.4% (at 14 min). Furthermore, the release rate of DOX from **G**-CuS-DOX becomes faster by increasing the intensity of the 915-nm laser (Figure S9, Supporting Information). This controllable release results from the fact that CuS in the **G**-CuS-DOX nanocapsules converts the 915-nm laser energy to heat and then confers the temperature elevation, leading to dissociation of the electrostatic interactions between DOX and **G**-CuS and controlled volume-shrinkage of **G**-CuS (Figure 2a and Figure S10, Supporting Information).[10a,13b] It is well known that the drug release ideally is carried out by controllably switching on or off the drug supply in order to maintain the active drug at the appropriate concentration in vivo for the required time to produce a continuous therapeutic effect. To realize the on/off release, we investigated the effects of the irradiation–non-irradiation cycle number on the DOX release, by irradiating **G**-CuS-DOX solutions (10 mg mL^{-1}, LC_{DOX} = 1%) with a 915-nm laser (1.6 W cm^{-2}) for 5 min each hour (Figure 2d). Without any irradiation of the laser, the cumulative release of DOX from **G**-CuS-DOX solution is only 8.2% at room temperature (RT) after 1 h, and it remains nearly unchanged during the next 4 h (A group). After the first 5-min irradiation (T > 42 °C) at 1 h, the cumulative release of DOX (B-D groups) increases remarkably to 27.4%, and remains almost unchanged during the subsequent non-irradiation term (at RT for 3 h, for the B group), indicating that 5-min on/long-time off release behavior takes place. Similarly, after the second 5-min irradiation (T > 42 °C) at 2 h, an obvious increase in the cumulative DOX release is obtained (groups C and D), i.e., the release percentage increases to 41.6%, and then remains nearly the same in the non-irradiation term (at RT for 2 h, for group C). Lastly, the third 5-min irradiation (T > 42 °C) at 3 h leads to a slight rise of released DOX to 46.3%, which then also remains unchanged during the following non-irradiation term (at RT). This irradiation-induced increase implies the switch-on effect in the DOX release, while the unchanged DOX content in the non-irradiation term indicates the switch-off effect for the DOX release. The present NIR-laser-switched release process should be attributed to the controllable temperature cycle (above or below 42 °C) of the **G**-CuS-DOX solution (Figure 2a), which is different from the traditional endogenous[1,2] or exogenous[3–7,24] stimuli-responsive nanocarriers that usually are spontaneous and/or cannot be shut off. Based on the above DOX-release results, one can conclude that the release of DOX from **G**-CuS-DOX nanocapsules can be efficiently controlled (turning on/off, rate adjustment, etc.) by 915-nm laser irradiation (on/off mode of the irradiation time, power control), revealing a unique and intelligent release mode.

Ideal nanocomposites must be nontoxic for biological applications. The cytotoxicity of **G**-CuS and **G**-CuS-DOX were evaluated by a cell counting kit-8 (CCK-8) assay with human hepatocarcinoma cells SMMC-7721 (7721 cells) and benign prostatic hyperplasia epithelial cell line (BPH-1 cells). The results confirm that both **G**-CuS and **G**-CuS-DOX aqueous dispersions have very low cytotoxicity (Figure S11, Supporting Information).

To investigate the combined photothermal/chemotherapy effects in vitro from **G**-CuS-DOX, the 7721 cell viability was measured after incubation with **G**-CuS-DOX (10 mg mL^{-1}; LC_{DOX} = 1%) under laser irradiation at 915 nm. For systematic comparison, we also investigated the single chemotherapy effects for free DOX (100 μg mL^{-1}) and "delivery DOX" (which is DOX that is only released from **G**-CuS-DOX), and single photothermal therapy from **G**-CuS nanocomposites (10 mg mL^{-1}, **Figure 3**). Obviously, free DOX shows a high pharmaceutical activity, i.e., less than 40% of the cells survive (Figure 3a). Without the irradiation of the NIR laser, all the experimental groups, including **G**-CuS, the delivery DOX, and **G**-CuS-DOX, show high cell viability (>90%) (Figure 3a), and the heating-delivery DOX from **G**-CuS-DOX at 37–42 °C also exhibits high cell viability (>80%) (Figure S12, Supporting Information), demonstrating the low cytotoxicity and high stability of **G**-CuS-DOX. It should be pointed out that although a small amount of DOX could be spontaneously released from the **G**-CuS-DOX group (without NIR laser, Figure 2c), the much lower dose of DOX cannot effectuate effective inhibition of cancer cell growth (Figure 3a and Figure S12, Supporting Information). With an increase of the laser intensity from 1.2 to 2.4 W cm^{-2}, the temperature of the **G**-CuS aqueous dispersion increases from 42 to 50 °C (inset in Figure 3a), and the **G**-CuS+NIR group causes a remarkably lower cell viability (such as, P < 0.01 for 2.0 versus 0 W cm^{-2}), verifying the photothermal therapy effects of **G**-CuS. Similarly, with the increase of the laser intensity from 1.2 to 2.4 W cm^{-2}, the cell viability from the delivery DOX group sharply decreases (such as, P < 0.05 for 2.0 versus 0 W cm^{-2}, Figure 3a). These results can be attributed to the fact that a higher laser intensity or more irradiation–non-irradiation cycle numbers results in a larger release of DOX from the **G**-CuS-DOX solution, as demonstrated in Figure S9, Supporting Information and Figure 2d, which brings about a better chemotherapeutic effect. Importantly, for the **G**-CuS-DOX+NIR group, the cell viability decreases remarkably with an intensity increase from 1.2 to 2.4 W cm^{-2} (such as, P < 0.01 for 2.0 versus 0 W cm^{-2}). In particular, when the laser intensity reaches to 2.0 or 2.4 W cm^{-2}, the **G**-CuS-DOX+NIR group reveals the lowest cell viability (versus delivery DOX or **G**-CuS+NIR, P < 0.05 for 2.0 W cm^{-2}; P < 0.01 for 2.4 W cm^{-2}) among all these groups (Figure 3a), owing to the synergic photothermal/chemotherapy effect, which is much higher than either the single photothermal therapy effect or the chemotherapy effect.

When the 915-nm laser intensity reaches or exceeds 2.4 W cm^{-2}, the solution remains at high temperature (≥50 °C), and long-time (≥8 min) irradiation would cause the inactivation of the released DOX (such as P < 0.01 for 8 min versus

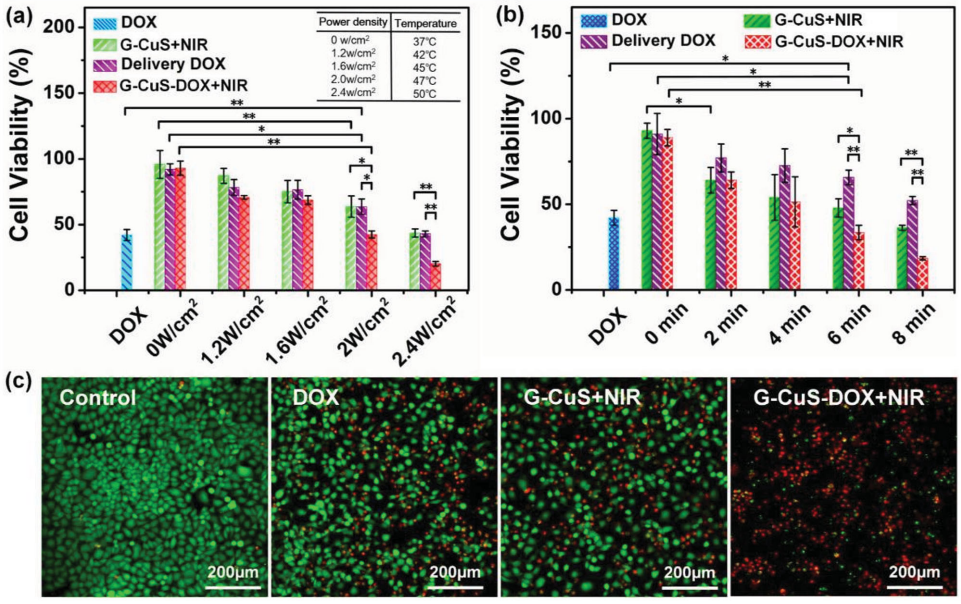

Figure 3. Therapy effects in vitro. a) Cell viability values (%) from free DOX (100 μg mL^{-1}), the "delivery DOX" (released from 10 mg mL^{-1} **G**-CuS-DOX by NIR laser), **G**-CuS (10 mg mL^{-1}) and **G**-CuS-DOX (10 mg mL^{-1}, LC_{DOX} = 1%) under irradiation of a 915 nm laser at different intensities (0–2.4 W cm^{-2}) for 5 min. b) Cell viability values (%) from different groups under the 915 nm laser irradiation at an intensity of 2.0 W cm^{-2} for various irradiation times (0–8 min). c) The confocal images of the 7721 cells from the control group and the experimental groups. The data are shown as mean ± standard deviation of three experiments, *P < 0.05, ** P < 0.01.

free DOX (see Figure S13, Supporting Information)). Thus, 915-nm laser irradiation at an intensity of 2.0 W cm^{-2} was selected for the later cell experiments. Subsequently, the effects of irradiation time (0–8 min) on cell viability were also studied (Figure 3b). With the increase of irradiation time to 6–8 min, the cell viability of the **G**-CuS-DOX+NIR group decreases (such as P < 0.01 for 6 versus 0 min), and is actually the lowest among all these groups at the same irradiation time (versus DOX delivery P < 0.05, or **G**-CuS+NIR P < 0.01 at 6 min). Simultaneously, to visually evaluate the viability difference in cellular level, the cells from different groups (control, free DOX, **G**-CuS+NIR, and **G**-CuS-DOX+NIR) were stained with calcein-AM and ethidium homodimer-1 to distinguish live (green) and dead (red) cells (Figure 3c). The majority of dead cells is observed in the **G**-CuS-DOX+NIR group, which is consistent with the previous CCK-8 assay of the cell proliferation rate. All these results show that **G**-CuS-DOX exhibits excellent synergic photothermal/chemotherapy effects that can be switched on controllably and adjusted by the irradiation intensity and time of the ex vivo NIR laser.

Based on their synergic photothermal/chemotherapy in vitro, **G**-CuS-DOX nanocapsules may have great potential as novel nanoagents for the therapy of tumors in vivo. Firstly, we investigated the on/off release behavior of DOX in tumor tissue. A **G**-CuS-DOX solution was injected into the SMMC-7721 tumor in mice. After 30 min, we find that the content of **G**-CuS-DOX and/or DOX in the blood is very low (all <0.3%) in the absence of an NIR laser, indicating that negligible spontaneous release of DOX into the blood occurs (Figure S14a, Supporting Information). Subsequently, the tumors were irradiated by a 915-nm laser (2.0 W cm^{-2}) for 10 min (temperature maintained at 47 °C). The cumulative release of DOX in the tumor increases to 55.14%, indicating that the release of DOX from **G**-CuS-DOX nanocapsules in tumor can be efficiently controlled by the 915-nm laser (Figure S14b, Supporting Information). It should be noted that pathological processes will not cause the pre-release of DOX from nanocapsules (Figure S15, Supporting Information).

To investigate their immediate therapy, tumors were injected with **G**-CuS and **G**-CuS-DOX solution, and then irradiated by the 915-nm laser (2.0 W cm^{-2}) for 10 min (T = 47 °C) at 24 h post-injection. After 48 h, the combined therapy effects were evaluated by ultrasound (US) imaging. For comparison, tumors were injected with PBS, **G**-CuS, or **G**-CuS-DOX without NIR laser irradiation under otherwise identical conditions, and the therapy effects were also estimated by US imaging. Obviously, US images from the flow-mode cannot visualize blood flow in tumors due to their small size (Figure S16, Supporting Information, upper row, yellow circles), while from B-mode US images the surface of the tumors can be distinguished from the soft tissue in mice, but the interior cannot be visualized (Figure S16, Supporting Information, middle row, yellow circles). Subsequently, the mice from all groups were injected with the contrast agent via retro-orbital injection (ROI) to further analyze the inside of the tumor, after which the increased US contrast images were observed in vivo under US contrast-mode (**Figure 4**a). For mice injected with PBS, **G**-CuS, and **G**-CuS-DOX without NIR laser irradiation, the complete power Doppler enhancement occurs immediately, following slow infusion of the contrast media, and prominent color flare is observed homogeneously throughout the entire tumors (Figure 4a, yellow circles).[25] However, for **G**-CuS+NIR and **G**-CuS-DOX+NIR groups, the contrast agents cannot completely perfuse the tumor, forming black defects (Figure 4a yellow or red

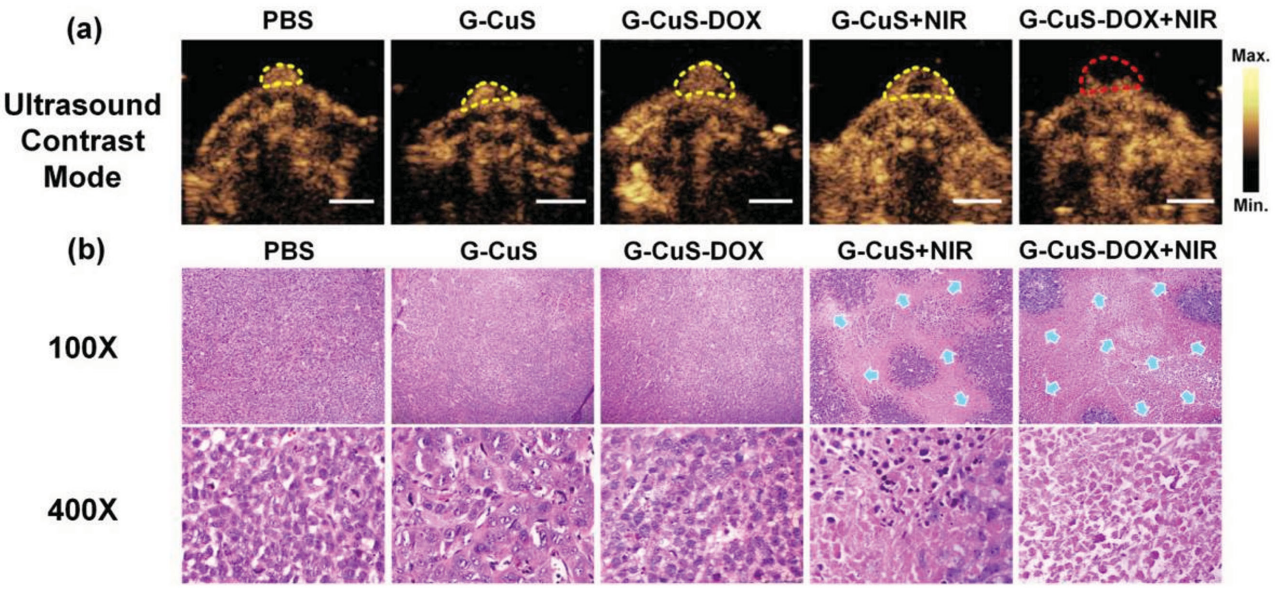

Figure 4. Immediate therapy effects in vivo. a) In vivo ultrasound images in contrast mode of the tumor-bearing mice from different groups (PBS, **G**-CuS, **G**-CuS-DOX, **G**-CuS+NIR laser, **G**-CuS-DOX+NIR laser); circles: tumor; scale bar: 5 mm. b) H&E-stained tumor sections collected from these groups; arrows: damaged areas for cells. The magnifications are 100× (middle row) and 400× (lower row).

circle), which potentially reveals the presence of a necrotic core within the tumors. To further evaluate the therapy effect, mice from different groups were scarified, and tumors were collected and fixed for histological analysis, as shown in H&E-stained images (H&E: hematoxylin/eosin) (Figure 4b). For PBS, **G**-CuS, and **G**-CuS-DOX groups without NIR laser irradiation, cells in their tumors mostly retain their normal morphology with apparent membrane and nuclear structure. Importantly, for the **G**-CuS+NIR group after NIR laser irradiation, several segmental damaged areas are observed at 100× magnification (arrows) and a section of pyknotic cells or cytolysis are revealed at 400× magnification, indicating that part of the cancer cells in the mice from the **G**-CuS+NIR group have been destroyed (Figure 4b). Furthermore, for the **G**-CuS-DOX+NIR group, one can find the largest damaged areas for 100× magnification (arrows), and a majority of the cancer cells are severely necrotized. In particular, from the image at 400× magnification, the maximum cytolysis and the loss of cell morphology are clearly observed. These data verify that **G**-CuS-DOX nanocapsules possess the most excellent immediate effects for in vivo therapy.

It is common knowledge that the metastatic spread of cancer cells is directly or indirectly responsible for more than 90% of cancer deaths,[26] therefore, it is of great importance to restrain metastatic tumors. For subcutaneous transplanted SMMC-7721 tumors, the cancer cells would be prone to spread to the liver to generate liver metastasis. Therefore, we analyzed the number of metastatic tumor nodules in livers and the tumor volume from different groups at 7 days post-treatment (**Figure 5**a,b, and Figure S17 and S18, Supporting Information). For PBS, **G**-CuS, **G**-CuS-DOX and the DOX group, tumors almost remain at their original diameter (Figure S17, Supporting Information). In addition, in livers from these four groups, there are numerous off-white suspected metastatic tumor nodules; no significant differences in nodule number can be found among these four groups (Figure 5a,b and Figure S18, Supporting Information). These suspected metastatic tumor nodules were confirmed by histopathology (H&E slices). These data reveal that the growth/metastasis of tumors cannot be inhibited after 7 days by the materials alone and/or DOX without NIR laser irradiation. In contrast, for the **G**-CuS+NIR group, the growth of tumors shows a significant inhibition after 7 days (versus PBS or **G**-CuS, all $P < 0.01$), and there are fewer metastatic tumor nodules in the livers (versus PBS or **G**-CuS, all $P < 0.01$; Figure 5a,b, Figure S17 and S18, Supporting Information). This finding demonstrates that the growth and metastasis of tumors have been partly inhibited by the photothermal effects from **G**-CuS. More importantly, for the **G**-CuS-DOX+NIR group, the growth of tumors also suffers a similar inhibition (versus PBS or **G**-CuS-DOX $P < 0.01$; versus DOX $P < 0.05$), while almost no metastatic tumor nodules are observed (versus PBS, **G**-CuS-DOX, DOX $P < 0.01$; versus **G**-CuS+NIR $P < 0.05$, Figure 5a,b and Figure S18, Supporting Information). Therefore, the metastasis of tumors can be efficiently inhibited by **G**-CuS-DOX nanocapsules with an NIR laser due to the synergic photothermal/chemotherapy effects.

To kill the tumors in mice, we carried out a long-term therapy for the **G**-CuS-DOX+NIR group. For comparison, tumors from **G**-CuS-DOX, DOX and the **G**-CuS+NIR groups were also studied (Figure 5c–f). For the **G**-CuS-DOX group (without laser irradiation), the tumor volume remains almost unchanged during the first ten days, but boosts rapidly in the subsequent term (from 10 to 24 days, Figure 5c,d). In addition, for **G**-CuS+NIR or DOX groups, the tumor volume shows an obvious decrease during the first ten days, but recurrent growth occurs from 10 to 24 days (DOX versus **G**-CuS-DOX $P < 0.05$, **G**-CuS+NIR versus **G**-CuS-DOX $P < 0.01$). In discrepancy with the other three groups, the volume of the tumors from the **G**-CuS-DOX+NIR group shows a continuous decrease and the

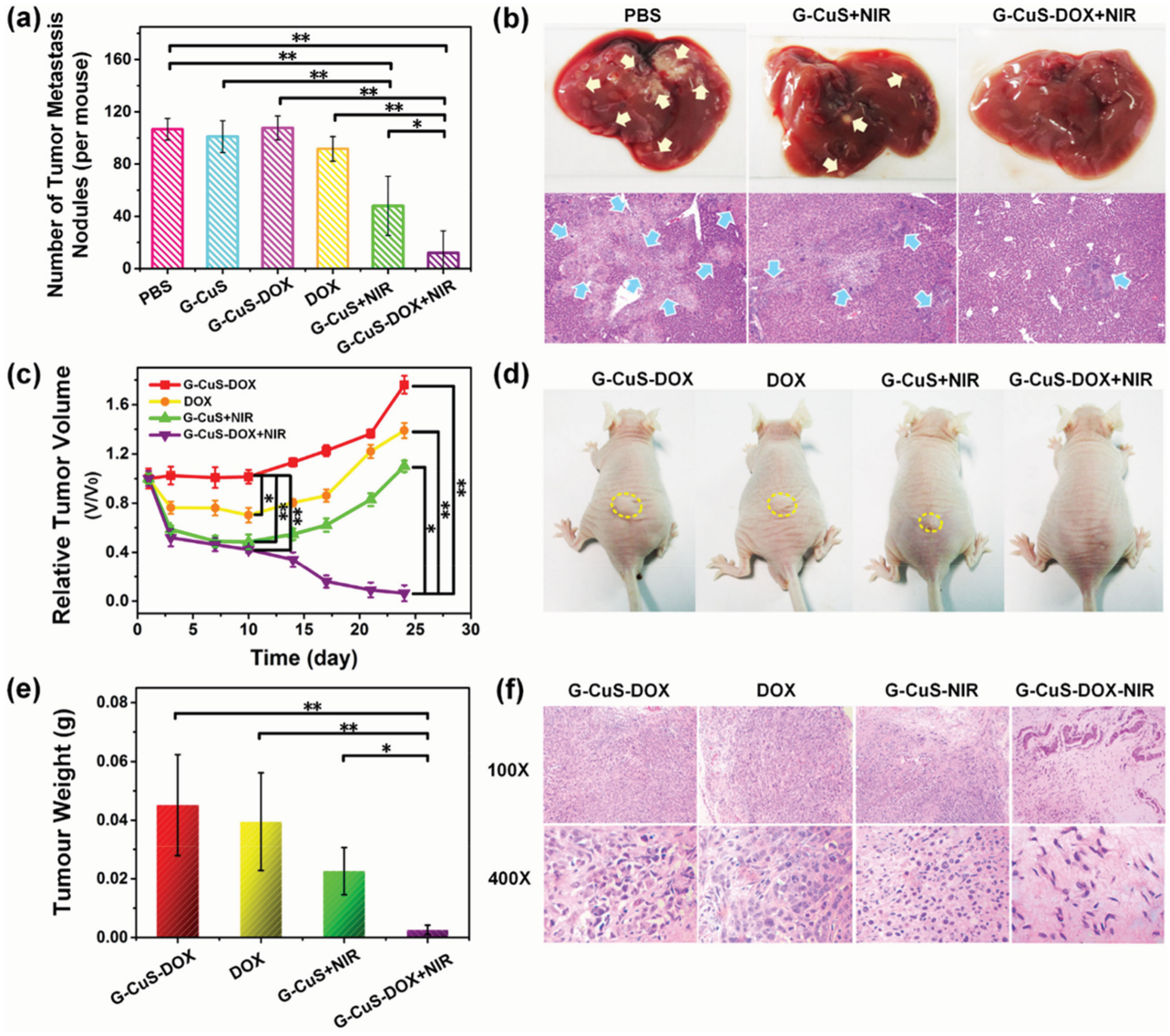

Figure 5. a,b) Analysis of tumor metastases to livers from different groups at 7 days post-treatment in vivo: a) the quantification of average liver metastases tumor nodules per mouse; b) representative photos of liver and H&E-stained liver slices, arrows: metastases tumor nodules (yellow), metastases area (blue). c–f) Therapy effects in vivo during 24 days: c) tumor growth curves from different groups; d) tumors from mice (yellow circles) at 24 days, e) average weights of the tumors and f) H&E-stained tumor slices from different groups at 24 days. Data represented as the mean ± standard deviation of six mice, $*P < 0.05$, $**P < 0.01$.

trend suggests an elimination at 24 days post-treatment (all $P < 0.05$, Figure 5c,d). The animals were sacrificed at 24 days post-treatment. Tumors were collected and weighed, and the results were consistent with the tumor volume (Figure 5e). Finally, the slices from the tumors were stained with H&E (Figure 5f). Evidently, the H&E images from **G**-CuS-DOX+NIR group confirm that cancer cells have suffered the most serious fibrosis compared with the other three groups, in which the cellular morphology has almost disappeared and a great number of nuclei have been dissolved (Figure 5f). Partial fibrosis is observed in the **G**-CuS+NIR group, and fewer are observed in the **G**-CuS-DOX and DOX groups.

The differences in therapeutic effects among these groups have also been analyzed. On the one hand, DOX, as a chemotherapeutic agent for SMMC-7721 tumors, will not show satisfying anticancer treatment effects if multiple and high dosages are not supplied for long periods.[10b] As a result, in the initial term of one-time DOX treatment, the inhibition of tumor growth emerges, while it relapses ultimately, as revealed in the tumor change from DOX group. On the other hand, although the one-time photothermal therapy can inhibit the tumor growth in the initial period, recurrent tumor growth occurs in the later period due to the disappearance of the therapy effects without NIR laser irradiation, as confirmed by the **G**-CuS+NIR group. In contrast, for the **G**-CuS-DOX+NIR laser group, ex vivo 915 nm laser irradiation as exogenous stimulus can be converted into in vivo heat (as endogenous stimulus), inducing a rapid increase of the tumor temperature (i.e., above 42 °C),

resulting in photothermal ablation of cancer cells in vivo. Simultaneously, a higher temperature (i.e., higher than the LCST) would release the "switch" of responsive nanocapsules to release DOX, resulting in continuous chemotherapy effects. Therefore, **G**-CuS-DOX nanocapsules show excellent synergic photothermal/chemotherapy effects for cancer cells in vivo under irradiation of an NIR laser, far exceeding the effects from photothermal therapy or chemotherapy alone. Furthermore, it is expected that, if part of the **G**-CuS-DOX nanocapsules is captured by normal tissues (such as liver and kidney), the photothermal effect cannot be produced and thus almost no drug can be released in the absence of an NIR laser, thus avoiding unpleasant side-effects successfully.

In summary, **G**-CuS-DOX nanocapsules have been designed and synthesized to serve as a new type of "smart nanobiomaterial". Under irradiation of an NIR laser, a solution of nanocapsules (Cu: 10–120 ppm) exhibits a rapid temperature elevation from 34 to 57 °C in 5 min due to efficient photothermal effects of the CuS nanoparticles. Simultaneously, higher temperatures (i.e., higher than the LCST) result in shrinkage of the nanocapsules, leading to the controllable release of DOX. However, if the NIR laser is switched off, the solution temperature decreases again, leading to interruption of both photothermal and chemotherapeutic effects. Moreover, when the nanocapsule solution is injected into the tumor of the mice, the temperature elevation and DOX release in the tumor can be switched on/off by the ex vivo NIR laser, for controllable and efficient synergistic photothermal/chemotherapy for the tumor. Therefore, the demonstrated intratumor injection of smart **G**-CuS-DOX nanocapsules provides a versatile and efficient method for future tumor therapy, but we anticipate that this method can also be extended to intravenous injection of the nanocapsules after conjugation of the target molecules.

Supporting Information

Supporting Information is available from the Wiley Online Library or from the author.

Acknowledgements

Z.Q.M. and F.W. contributed equally to this work. This work was financially supported by the National Natural Science Foundation of China (Grant No. 50925312, 51272299, 51273040, 51473033), Program for Changjiang Scholars and Innovative Research Team in University (Grant No. IRT1221, T2011079), High-Tech Research and Development Program of China (Grant No. 2012AA030309), Project of the Shanghai Committee of Science and Technology (13JC1400300), Innovation Program of Shanghai Municipal Education Commission (Grant No. 13ZZ053), Shanghai Leading Academic Discipline Project (Grant No. B603). The authors are grateful for the assistance from the Experimental Research Center of the First People's Hospital, Shanghai Jiaotong University, and from Dr. Eric Habib for revising the manuscript. Animal experiments were performed according to the Guidelines for institutional committee for animal use and care regulations.

Received: June 4, 2015
Revised: September 23, 2015
Published online: November 9, 2015

[1] a) Y. Qiu, K. Park, *Adv. Drug Delivery Rev.* **2001**, *53*, 321; b) Z. Deng, Z. Zhen, X. Hu, S. Wu, Z. Xu, P. K. Chu, *Biomaterials* **2011**, *32*, 4976.
[2] L. Zhu, P. Kate, V. P. Torchilin, *ACS Nano* **2012**, *6*, 3491.
[3] a) M. Yatvin, J. Weinstein, W. Dennis, R. Blumenthal, *Science* **1978**, *202*, 1290; b) K. J. Chen, H. F. Liang, H. L. Chen, Y. Wang, P. Y. Cheng, H. L. Liu, Y. Xia, H. W. Sung, *ACS Nano* **2012**, *7*, 438.
[4] a) S. I. Jenkins, M. R. Pickard, N. Granger, D. M. Chari, *ACS Nano* **2011**, *5*, 6527; b) S. Louguet, B. Rousseau, R. Epherre, N. Guidolin, G. Goglio, S. Mornet, E. Duguet, S. Lecommandoux, C. Schatz, *Polym. Chem.* **2012**, *3*, 1408.
[5] N. Y. Rapoport, A. M. Kennedy, J. E. Shea, C. L. Scaife, K.-H. Nam, *J. Controlled Release* **2009**, *138*, 268.
[6] V. Shanmugam, S. Selvakumar, C.-S. Yeh, *Chem. Soc. Rev.* **2014**, *43*, 6254.
[7] H. Kim, S.-M. Jeong, J.-W. Park, *J. Am. Chem. Soc.* **2011**, *133*, 5206.
[8] S. Mura, J. Nicolas, P. Couvreur, *Nat. Mater.* **2013**, *12*, 991.
[9] Z. Chen, L. Zhang, Y. Sun, J. Hu, D. Wang, *Adv. Funct. Mater.* **2009**, *19*, 3815.
[10] a) Z. Sheng, D. Hu, M. Zheng, P. Zhao, H. Liu, D. Gao, P. Gong, G. Gao, P. Zhang, Y. Ma, L. Cai, *ACS Nano* **2014**, *8*, 12310; b) M. Zheng, C. Yue, Y. Ma, P. Gong, P. Zhao, C. Zheng, Z. Sheng, P. Zhang, Z. Wang, L. Cai, *ACS Nano* **2013**, *7*, 2056.
[11] a) J. Chen, M. Yang, Q. Zhang, E. C. Cho, C. M. Cobley, C. Kim, C. Glaus, L. V. Wang, M. J. Welch, Y. Xia, *Adv. Funct. Mater.* **2010**, *20*, 3684; b) M.-F. Tsai, S.-H. G. Chang, F.-Y. Cheng, V. Shanmugam, Y.-S. Cheng, C.-H. Su, C.-S. Yeh, *ACS Nano* **2013**, *7*, 5330; c) J. Nam, W.-G. La, S. Hwang, Y. S. Ha, N. Park, N. Won, S. Jung, S. H. Bhang, Y.-J. Ma, Y.-M. Cho, M. Jin, J. Han, J.-Y. Shin, E. K. Wang, S. G. Kim, S.-H. Cho, J. Yoo, B.-S. Kim, S. Kim, *ACS Nano* **2013**, *7*, 3388; d) X. Huang, S. Tang, X. Mu, Y. Dai, G. Chen, Z. Zhou, F. Ruan, Z. Yang, N. Zheng, *Nat. Nanotechnol.* **2011**, *6*, 28.
[12] a) M. Li, X. Yang, J. Ren, K. Qu, X. Qu, *Adv. Mater.* **2012**, *24*, 1722; b) A. L. Antaris, J. T. Robinson, O. K. Yaghi, G. Hong, S. Diao, R. Luong, H. Dai, *ACS Nano* **2013**, *7*, 3644; c) Z. Sheng, L. Song, J. Zheng, D. Hu, M. He, M. Zheng, G. Gao, P. Gong, P. Zhang, Y. Ma, L. Cai, *Biomaterials* **2013**, *34*, 5236.
[13] a) Y. Li, W. Lu, Q. Huang, C. Li, W. Chen, *Nanomedicine* **2010**, *5*, 1161; b) T. Liu, C. Wang, X. Gu, H. Gong, L. Cheng, X. Shi, L. Feng, B. Sun, Z. Liu, *Adv. Mater.* **2014**, *26*, 3433.
[14] a) Q. Tian, F. Jiang, R. Zou, Q. Liu, Z. Chen, M. Zhu, S. Yang, J. Wang, J. Wang, J. Hu, *ACS Nano* **2011**, *5*, 9761; b) Q. Tian, M. Tang, Y. Sun, R. Zou, Z. Chen, M. Zhu, S. Yang, J. Wang, J. Wang, J. Hu, *Adv. Mater.* **2011**, *23*, 3542; c) Q. Tian, J. Hu, Y. Zhu, R. Zou, Z. Chen, S. Yang, R. Li, Q. Su, Y. Han, X. Liu, *J. Am. Chem. Soc.* **2013**, *135*, 8571.
[15] a) Z. Chen, Q. Wang, H. Wang, L. Zhang, G. Song, L. Song, J. Hu, H. Wang, J. Liu, M. Zhu, D. Zhao, *Adv. Mater.* **2013**, *25*, 2095; b) W. Xu, Q. Tian, Z. Chen, M. Xia, D. K. Macharia, B. Sun, L. Tian, Y. Wang, M. Zhu, *J. Mater. Chem. B* **2014**, *2*, 5594.
[16] a) A. Agarwal, M. A. Mackey, M. A. El-Sayed, R. V. Bellamkonda, *ACS Nano* **2011**, *5*, 4919; b) L. J. E. Anderson, E. Hansen, E. Y. Lukianova-Hleb, J. H. Hafner, D. O. Lapotko, *J. Controlled Release* **2010**, *144*, 151.
[17] a) Y. T. Chang, P. Y. Liao, H. S. Sheu, Y. J. Tseng, F. Y. Cheng, C. S. Yeh, *Adv. Mater.* **2012**, *24*, 3309; b) T. Shang, C.-d. Wang, L. Ren, X.-h. Tian, D.-h. Li, X.-b. Ke, M. Chen, A.-q. Yang, *Nanoscale Res. Lett.* **2013**, *8*, 1; c) G. Song, Q. Wang, Y. Wang, G. Lv, C. Li, R. Zou, Z. Chen, Z. Qin, K. Huo, R. Hu, J. Hu, *Adv. Funct. Mater.* **2013**, *23*, 4280.
[18] a) M. S. Yavuz, Y. Cheng, J. Chen, C. M. Cobley, Q. Zhang, M. Rycenga, J. Xie, C. Kim, K. H. Song, A. G. Schwartz, L. V. Wang, Y. Xia, *Nat. Mater.* **2009**, *8*, 935; b) W. Wu, J. Shen, P. Banerjee, S. Zhou, *Biomaterials* **2010**, *31*, 7555; c) X.-q. Zhao, T.-x. Wang, W. Liu, C.-d. Wang, D. Wang, T. Shang, L.-h. Shen, L. Ren,

J. Mater. Chem. **2011**, *21*, 7240; d) H. Wan, Y. Zhang, Z. Liu, G. Xu, G. Huang, Y. Ji, Z. Xiong, Q. Zhang, J. Dong, W. Zhang, H. Zou, *Nanoscale* **2014**, *6*, 8743.

[19] a) J. Lutz, Ö. Akdemir, A. Hoth, *J. Am. Chem. Soc.* **2006**, *128*, 13046; b) S. Sun, P. Wu, *Macromolecules* **2013**, *46*, 236; c) M. Xia, Y. Cheng, Z. Meng, X. Jiang, Z. Chen, P. Theato, M. Zhu, *Macromol. Rapid Commun.* **2015**, *36*, 477.

[20] a) A. Silvestre Bongiovanni, A. M. María, R. R. Claudia, J. K. Marcelo, A. B. Cesar, *Nanotechnology* **2014**, *25*, 495602; b) Y. Pei, M.-Y. Wei, B. Cheng, Y. Liu, Z. Xie, K. Nguyen, B. Yuan, *Sci. Rep.* **2014**, *4*.

[21] H. Wang, J. Yi, S. Mukherjee, P. Banerjee, S. Zhou, *Nanoscale* **2014**, *6*, 13001.

[22] a) C. Wang, H. Xu, C. Liang, Y. Liu, Z. Li, G. Yang, L. Cheng, Y. Li, Z. Liu, *ACS Nano* **2013**, *7*, 6782; b) A. V. Kabanov, S. V. Vinogradov, *Angew. Chem. Int. Ed.* **2009**, *48*, 5418.

[23] C. Fan, S. Wang, J. W. Hong, G. C. Bazan, K. W. Plaxco, A. J. Heeger, *Proc. Natl. Acad. Sci. USA* **2003**, *100*, 6297.

[24] S. R. Sershen, S. L. Westcott, N. J. Halas, J. L. West, *J. Biomed. Mater. Res.* **2000**, *51*, 293.

[25] Z. W. Xing, J. R. Wang, H. T. Ke, B. Zhao, X. L. Yue, Z. F. Dai, J. B. Liu, *Nanotechnology* **2010**, *21*, 145607.

[26] a) M. B. Sporn, *Ann. NY Acad. Sci.* **1997**, *833*, 137; b) C. Liang, S. Diao, C. Wang, H. Gong, T. Liu, G. Hong, X. Shi, H. Dai, Z. Liu, *Adv. Mater.* **2014**, *26*, 5646.